Mon. Not. R. Astron. Soc. **382,** 1447–1459 (2007) doi:10.1111/j.1365-2966.2007.12496.x

VLT/near-infrared integral field spectrometer observations of molecular hydrogen lines in the knots of the planetary nebula NGC 7293 (the Helix Nebula)⋆

M. Matsuura,[1,2,3]† A. K. Speck,[4] M. D. Smith,[5] A. A. Zijlstra,[3,6] S. Viti,[7] K. T. E. Lowe,[8] M. Redman,[9] C. J. Wareing[3] and E. Lagadec[3]

[1]*National Astronomical Observatory of Japan, Osawa 2-21-1, Mitaka, Tokyo 181-8588, Japan*
[2]*School of Mathematics and Physics, Queen's University of Belfast, Belfast BT7 1NN*
[3]*School of Physics and Astronomy, University of Manchester, Sackville Street, PO Box 88, Manchester M60 1QD*
[4]*Physics and Astronomy, University of Missouri, Columbia, MO 65211, USA*
[5]*Centre for Astrophysics and Planetary Science, School of Physical Sciences, The University of Kent, Canterbury CT2 7NH*
[6]*South African Astronomical Observatory, PO Box 9, 7935 Observatory, South Africa*
[7]*Department of Physics and Astronomy, University College London, Gower Street, London WC1E 6BT*
[8]*Science and Technology Research Centre, University of Hertfordshire, College Lane, Hatfield, Hertfordshire AL10 9AB*
[9]*Department of Physics, National University of Ireland Galway, Galway, Republic of Ireland*

Accepted 2007 September 18. Received 2007 September 6; in original form 2007 February 23

ABSTRACT

Knots are commonly found in nearby planetary nebulae (PNe) and star-forming regions. Within PNe, knots are often found to be associated with the brightest parts of the nebulae and understanding the physics involved in knots may reveal the processes dominating in PNe. As one of the closest PNe, the Helix Nebula (NGC 7293) is an ideal target to study such small-scale (∼300 au) structures. We have obtained infrared integral spectroscopy of a comet-shaped knot in the Helix Nebula using the Spectrograph for INtegral Field Observations in the Near Infrared (SINFONI) on the Very Large Telescope at high spatial resolution (50–125 mas). With spatially resolved 2-μm spectra, we find that the H_2 rotational temperature within the cometary knots is uniform. The rotational-vibrational temperature of the cometary knot (situated in the innermost region of the nebula, 2.5 arcmin away from the central star) is 1800 K, higher than the temperature seen in the outer regions (5–6 arcmin from the central star) of the nebula (900 K), suggesting that the excitation temperature varies across the nebula. The obtained intensities are reasonably well fitted with 27 km s^{-1} C-type shock model. This ambient gas velocity is slightly higher than the observed [He II] wind velocity of 13 km s^{-1}. The gas excitation can also be reproduced with a photon-dominant region (PDR) model, but this requires an order of magnitude higher ultraviolet radiation. Both models have limitations, highlighting the need for models that treat both hydrodynamical physics and the PDR.

Key words: circumstellar matter – ISM: clouds – ISM: jets and outflows – ISM: molecules – planetary nebulae: individual: NGC 7293 – infrared: stars.

1 INTRODUCTION

In recent years, it has become clear that knots of dense material are common in nebulae, including planetary nebulae (PNe; e.g. O'Dell et al. 2002) and star-forming regions (e.g. McCaughrean & Mac Low 1997). In one of the best-studied PN case, that of the Helix Nebula (NGC 7293), knots in the inner regions have a comet-like shape (O'Dell & Handron 1996) and are thus known as cometary knots. The Helix Nebula is estimated to contain more than 20 000 cometary-shaped knots (Meixner et al. 2005). The apparent commonality of occurrence in PNe of these knots has led to the assertion that all circumstellar nebulae are clumpy in structure (e.g. O'Dell et al. 2002; Speck et al. 2002; Matsuura et al. 2005b). As knots occupy the brightest parts of the PNe, understanding their physical nature is essential to understanding the dominant physics governing the nebula.

The origin of these knots remains unknown. The knots' form is also disputed: they may have been present during the preceding

⋆Based on observations with the European Southern Observatory, Very Large Telescope with an instrument, SINFONI (the proposal numbers: 076.D-0807).

†E-mail: mikako@optik.mtk.nao.ac.jp

asymptotic giant branch (AGB) phase (e.g. Dyson et al. 1989), or only have formed during the PN phase. The suggested formation mechanisms fall into two main scenarios. First, photoevaporation from condensations which pre-exist in the circumstellar envelope was considered. Speck et al. (2002) suggest that the ultraviolet (UV) radiation from the central star heats the surface of a condensation, emitting Hα and H_2 on the facing side. Secondly, the interaction of a fast stellar wind with the slowly expanding AGB wind, during the early stage of PN phase, has been considered (e.g Vishniac 1994; Pittard et al. 2005; García-Segura et al. 2006). Pittard et al. (2005) found that cometary knots may be formed through instabilities where a supersonic wind impacts a subsonic wind.

In addition to being seen as inhomogeneities within the ionized gas emission from nebulae, the knots also contain molecular gas (Speck et al. 2002, 2003). This yields a potential clue to their origin. Redman et al. (2003) argued that some molecular species formed in the AGB atmosphere can survive if molecules are shielded in clumps from UV radiations by extinction. However, if the knots (re-) form during the ionized PN phase, the earlier AGB molecules were photodissociated, and the molecules re-form within the knots, under conditions of relatively low density and higher UV intensity compared to the AGB wind. In these conditions, only simple molecules are expected to be present (Woods 2004).

Using seeing-limited observations (1.2 arcsec) of the $H_2 v = 1$–0 S(1) line in a single knot, Huggins et al. (2002) found H_2 gas in both the head and the tail of the knot, following the distribution of ionized gas traced by Hα and [N II]. In contrast, CO thermal emission was found to emanate only from the tail. Higher angular resolution images obtained with *HST* (Meixner et al. 2005) resolved the globular H_2 emission into crescent-shaped regions. With these previous studies, it is not clear whether the hydrogen molecules and ionized gas are co-located within the head or spatially separated.

The excitation mechanisms for molecular hydrogen in PNe have long been controversial, with contention between fluorescent/thermal excitation in photon-dominant regions (PDRs) and shock excitation. Tielens & Hollenbach (1985) and Black & van Dishoeck (1987) showed that vibrationally excited H_2 (by far-UV pumping) traces the surface of dense regions in the process of becoming photoionized. On the other hand, molecules can form in a post-shock region (Neufeld & Dalgarno 1989), and H_2 can be excited by shocks (Beckwith et al. 1980; Hollenbach & McKee 1989). The cooling region after the shock can be resolved if it is a C-type (continuous) shock, but the region is too small to be resolved for J-type (jump) shocks. A comparison of models with spatially resolved spectra, which covers multiple line ratios, will help to understand the excitation mechanism of H_2.

The Helix Nebula (NGC 7293) is one of the nearest PNe, with a largest diameter of more than half a degree (Hora et al. 2006) and a parallax distance of 219 pc (Harris et al. 2007). Because of its distance, small-scale structures inside the nebula are well resolved and this nebula is used as a proxy to understand the structures found in PNe.

Table 1. Observing log.

Target	Pixel-scale of the camera (mas^2)	Pixel-scale in reduced data (mas^2)	Exposure time	Telluric standard Name	Spectral type	K mag[a]
K1	125 × 250	125 × 125	300 s × 10 600 s × 10	Hip 115329	G2V	7.552 ± 0.017
	50 × 100	50 × 50	600 s × 10	Hip 023422	G2V	7.862 ± 0.017

[a] K mag: K'-band magnitudes from 2MASS.

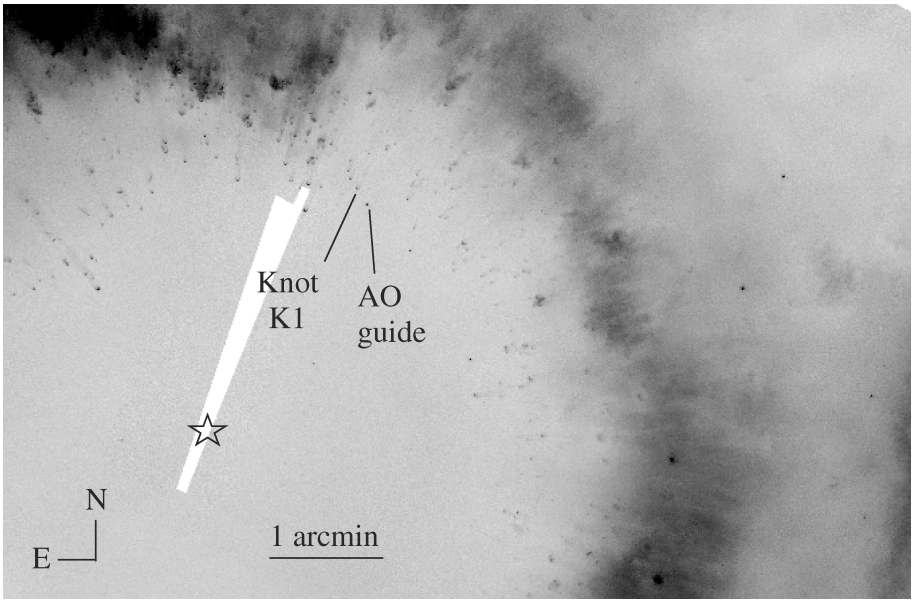

Figure 1. The location of the cometary knot K1 is plotted on the *F658N* ([N II] + Hα) image (O'Dell et al. 2004), together with the AO guide star. The star symbol indicates the place of the central star.

We have observed a cometary knot in the Helix Nebula, using the adaptive-optics-assisted, near-infrared integral field spectrometer on the Very Large Telescope (VLT). We have achieved 50–100 mas spatial resolution. Our data provide the first spatially resolved spectra within a knot at 2 μm and further this is the highest spatial resolution image + spectra of this PN at this wavelength. Our observations of H_2 spectral line ratios allow us to derive the excitation temperatures within the knot, as well as the possible excitation mechanisms of H_2.

2 OBSERVATIONS AND ANALYSIS

A knot in the Helix Nebula was observed by the Spectrograph for INtegral Field Observations in the Near Infrared (SINFONI; Eisenhauer et al. 2003; Bonnet et al. 2004) installed at the Cassegrain focus of the VLT. The grating for the *K* band was used. The wavelength band of the grating was mapped to the 2048 pixel detector in the dispersion direction. We used two plate-scales: the spatial resolutions are 125×250 and 50×100 mas^2. For all of the observations, a nearby star (RA = $22^h29^m33\overset{s}{.}017$, Dec. = $-20°48'12\overset{''}{.}68$ J2000) was used as an Adaptive Optics (AO) guide star. The spatial resolution is usually determined by the pixel-scale while using the 125×250 mas^2 plate-scale (i.e. the images are undersampled), while for the 50×100 mas^2 scale both the corrections of the AO system and the pixel-scale are important. The spectral resolutions $\lambda/\Delta\lambda$ are 4490 and 5090 for the 125×250- and 50×100-mas^2 cameras, respectively. The observing log is summarized in Table 1. The coordinates of our target knot K1 are $22^h29^m33\overset{s}{.}414$, $-20°48'04\overset{''}{.}73$ (J2000) measured from the data used by O'Dell, McCullough & Meixner (2004). This knot is noted as ID 6 in Meaburn et al. (1998) and is about 2.5 arcmin away from the central star (Fig. 1). It is located at the inner rim of the ring-shaped nebula filled with cometary knots.

The observing run was carried out on the first-half nights from 2005 November 2 to 4. The sky was clear on November 3, with occasional thin cloud passing on November 2 and 4. The telluric standards were observed immediately after the target. The telluric standard stars were used for flux and spectral-response calibration, as well as for the measurements of the point spread function (PSF). Model spectra from Pickles (1998) are used as template spectra for

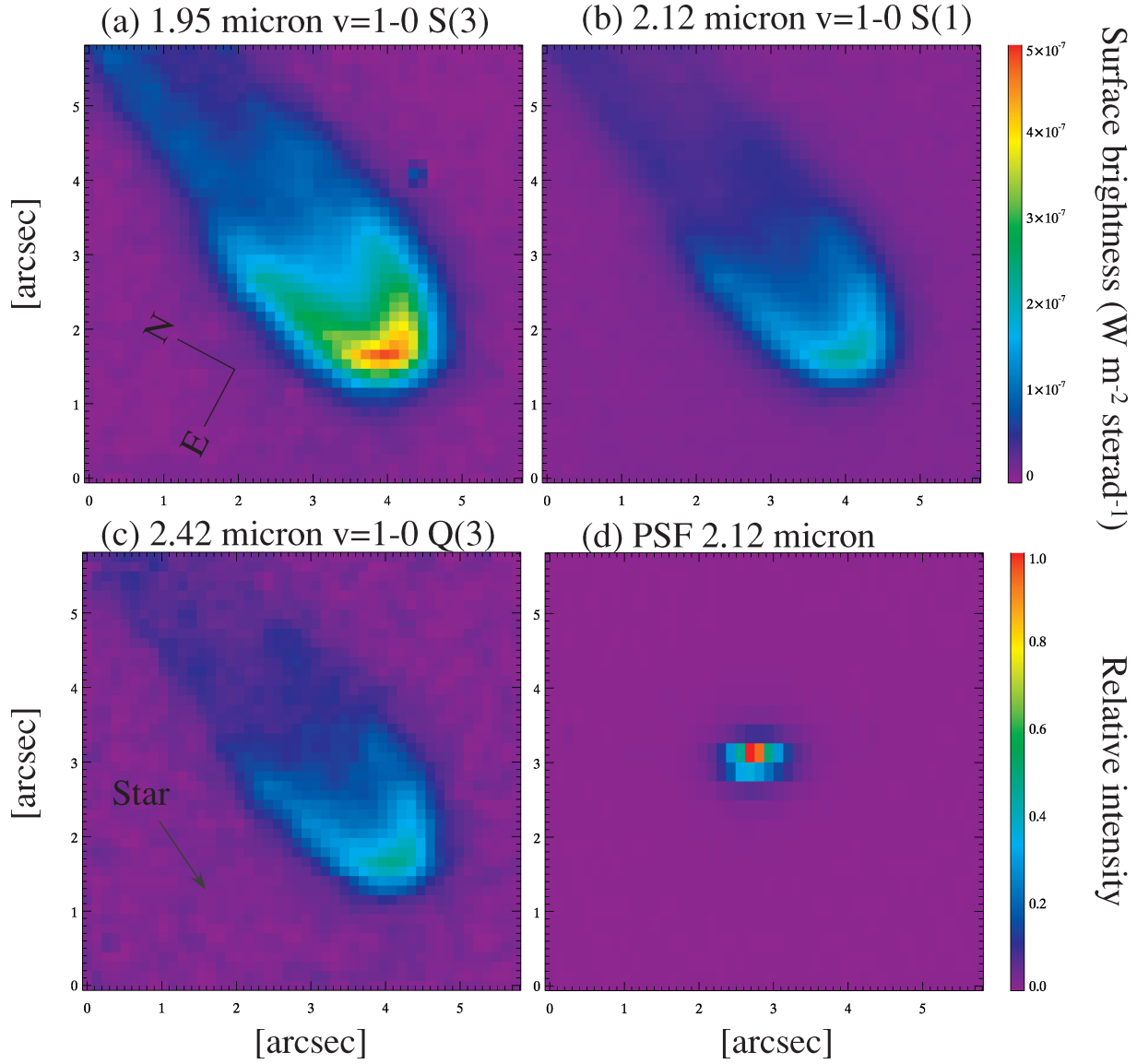

Figure 2. Images of the cometary knot K1, taken by the 250-mas camera. The PSF at 2.12 μm is found in (d). The direction of the central star is marked in (c).

the telluric standard stars. The wavelength resolution of the model spectra is 4000 only, but we assume that this difference in wavelength resolution is not critical for our analysis of the emission lines.

The field of view was slightly jittered to minimize the influence of bad pixels. The sky level was measured at +10 arcmin away in the declination direction, which is outside the bright part of the nebula. Some residual of the sky level was left, and we use the integral field to remove the residual sky level.

The European Southern Observatory (ESO) data-reduction pipeline for SINFONI on GASGANO (Modigliani et al. 2007) was used. Distortion-correction and flat-correction were adopted. Wavelength-calibration used the Ne and Ar wavelength lamps, linearly interpolated throughout the entire wavelength coverage. After the data reduction with GASGANO, the final pixel was resampled to a 125 and 50 mas scale for 125 × 250- and 50 × 100-mas^2 plate-scale images, respectively.

The absolute flux-calibration has some uncertainty, due to the possibility of occasional thin cirrus (up to 0.2 mag) and the generic difficulty in the calibration of diffuse intensity using an AO-assisted point source. We reduced two 125-mas target spectra using two different exposure times independently, and the final spectra and images were obtained by averaging these two data sets. The average of our measured flux over 2 × 2 arcsec^{-2} is 1.2 × 10^{-4} erg s^{-1} cm^{-2} sr^{-1}. Speck et al. (2002) gives the intensity of K1 at H_2 v = 1–0 S(1) as ∼5–10 × 10^{-5} erg s^{-1} cm^{-2} sr^{-1}; the knots are not fully resolved (2 arcsec pixel^{-1}) and the flux of this knot is close to the detection limit (∼1 × 10^{-4} erg s^{-1} cm^{-2} sr^{-1}). A knot in the outer regions of the Helix Nebula, with a similar flux level to our knot in Speck et al. (2002)'s measurements, was observed by Meixner et al. (2005). They find a surface brightness of H_2 of ∼1 × 10^{-4} erg s^{-1} cm^{-2} sr^{-1}. We conservatively adopt a systematic calibration uncertainty of 50 per cent. Further, the sky condition affects the correction of the atmospheric transmittance, especially shortward of 2 μm and longward of 2.4 μm, due to the variation in terrestrial H_2O. The relative intensities of lines below 2.0 μm and above 2.4 μm have an error of ∼30 per cent. We ignore the extinction at 2 μm; as discussed later, the extinction affects the absolute intensity less than 5 per cent ($A_{\lambda=2.128\,\mu m}$ = 0.05 mag).

3 DESCRIPTION OF THE DATA

3.1 Morphology

Fig. 2 shows the image of the cometary knot K1 as seen in the three strongest H_2 lines. The knot shows an elongated head with a narrower tail. The brightest emission is found in a crescent near the tip of the head. The crescent ends in two linear segments, indicated by the dotted lines in Fig. 3 on the 2.12 μm v = 1–0 S(1) image. These segments are not co-aligned and deviate from the direction of the narrower tail. Overall, this gives the impression of a 'tadpole' shape, as opposed to the cylindrical shape favoured by O'Dell & Handron (1996), although in either case the overall shape is largely axisymmetric. Both the linear segments and the tail are brighter on the eastern side of the knot.

The peak emission is located slightly behind the tip (Fig. 3). There is a faint nebulosity around the bright head. This faint nebulosity appears not to be the wing of the PSF. The faint halo extends along the linear segments where the peak emission is much fainter. The higher resolution image (50 mas pixel^{-1}) in Fig. 4 also shows this faint nebulosity, suggesting that at least part of this faint nebulosity is real.

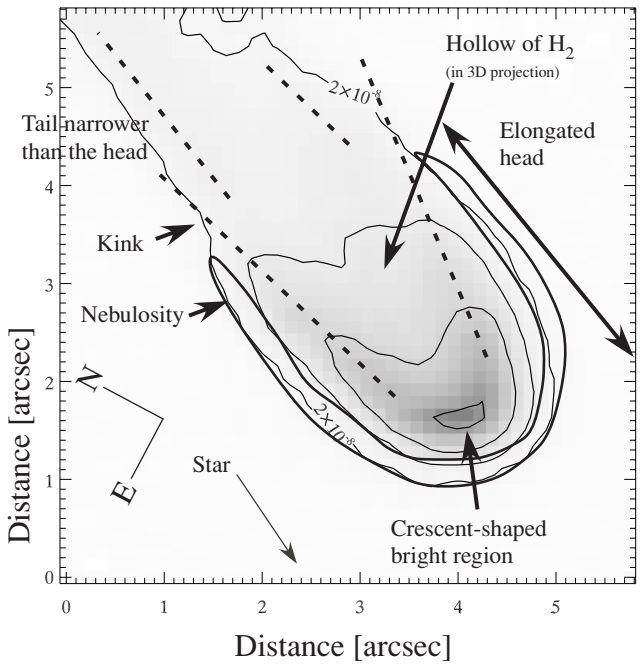

Figure 3. Annotated 2.12-μm image of the knot K1 (see the text for details).

The apparent diameter at the head is about 2.5 arcsec including the faint rim, while the diameter decreases to about 2 arcsec along the tail (Fig. 5). The transition from the linear segment to the narrower tail is visible as a kink, 2.8 arcsec from the head on the east side. It is less clearly visible on the west side.

3.1.1 *H_2 emission from the surface of knots*

The deconvolved image (Fig. 6) shows a limb-brightened head of the knot. Within the head there may be an H_2 empty region. Fig. 7 shows the radial cross-section of the head 1 arcsec inside from the brightest point. The intensity at the mid-point is about 65 per cent of the peak in the raw image and about 40 per cent in the deconvolved image. To demonstrate the shape, we modelled the radial profile in two dimensions, assuming a thin ring with a large hollow area inside (Figs 7b and c). The diameter of the circular ring is 1.5 arcsec. The density structure of the ring is assumed to be a Gaussian with a width of 0.075 arcsec. The radial cut in the deconvolved image is reasonably well reproduced by this model (Fig. 7a). The H_2 emitting region is probably a very thin surface of the knot, except at the tip.

3.1.2 *Comparisons with HST [N II] and [O III] images*

Fig. 8 shows the image of the knot K1 at 2.12 μm H_2 v = 1–0 S(1), with a comparison of *HST F658N* (mainly [N II] and some contribution of Hα) with *F502N* ([O III]) images from O'Dell et al. (2004). The precise alignment between SINFONI and *HST* images is unknown, and the images were registered such that the tip of the knot is located at the same place at [N II] and H_2 v = 1–0 S(1).

The [O III] image shows the knot in absorption; the tip is slightly off the peak from [N II] images (Fig. 9). This has also been found by O'Dell & Henney (2000) for other knots.

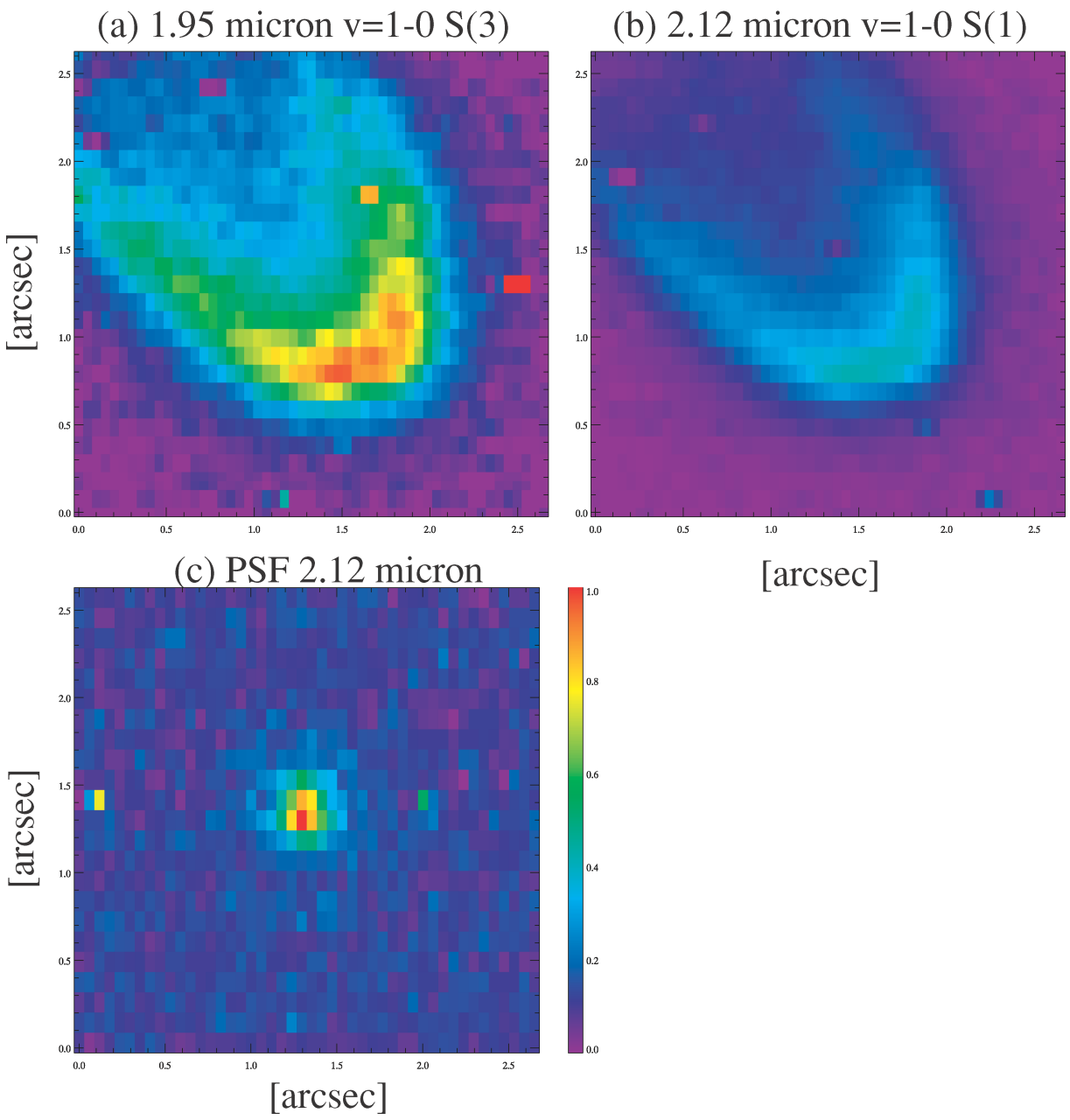

Figure 4. Image of the cometary knot K1, taken with the 100-mas camera. The PSF at 2.12 μm is found in (c).

A cross-section of the H_2 $v = 1$–0 S(1) and [N II] + Hα images shows that the decay of the intensities towards the tail is very fast (almost immediate) for the ionized lines, and slower for the H_2 $v = 1$–0 S(1). The main ionized region is a thin layer at the tip; the majority of the material remains molecular or neutral.

3.2 Spectra

Fig. 10 shows the spectra of the knot K1 at 12 regions indicated in Fig. 11. Within each region of 5 × 5 pixel (except region (a) which has 5 × 4 pixel), the SINFONI data have been averaged. At most 12 H_2 lines (three of them with low signal-to-noise ratio) are detected by SINFONI. The intensities are summarized in Table 2. The strongest detected line is the 1.95 μm H_2 $v = 1$–0 S(3), and the 2.12 μm H_2 $v = 1$–0 S(1) and 2.4 μm $v = 1$–0 Q branches are also strong. The H_2 lines are unresolved at the resolution of $R = 5090$. The 2.07 μm $v = 2$–1 S(3), 2.15 μm $v = 2$–1 S(2) and 2.20 μm $v = 3$–2 S(3) lines are only marginally detected.

Several high transition lines within this wavelength range are not detected, such as the 2.00 μm $v = 2$–1 S(4), 2.38 μm $v = 3$–2 S(1). The Brγ line is not detected.

3.2.1 Energy diagram

Fig. 12 shows the energy diagram of the H_2 lines for several regions in the knot indicated in Fig. 11. Einstein coefficients from Turner, Kirby-Docken & Dalgarno (1977) are used. The slopes in the diagrams show that the line intensities follow a $T = 1800$ K local thermodynamic equilibrium (LTE) distribution. At the bright area (a)–(c), the observed line intensities follow the 1800 K LTE line up to the upper energy of 8000 cm^{-1}. The systematic uncertainty

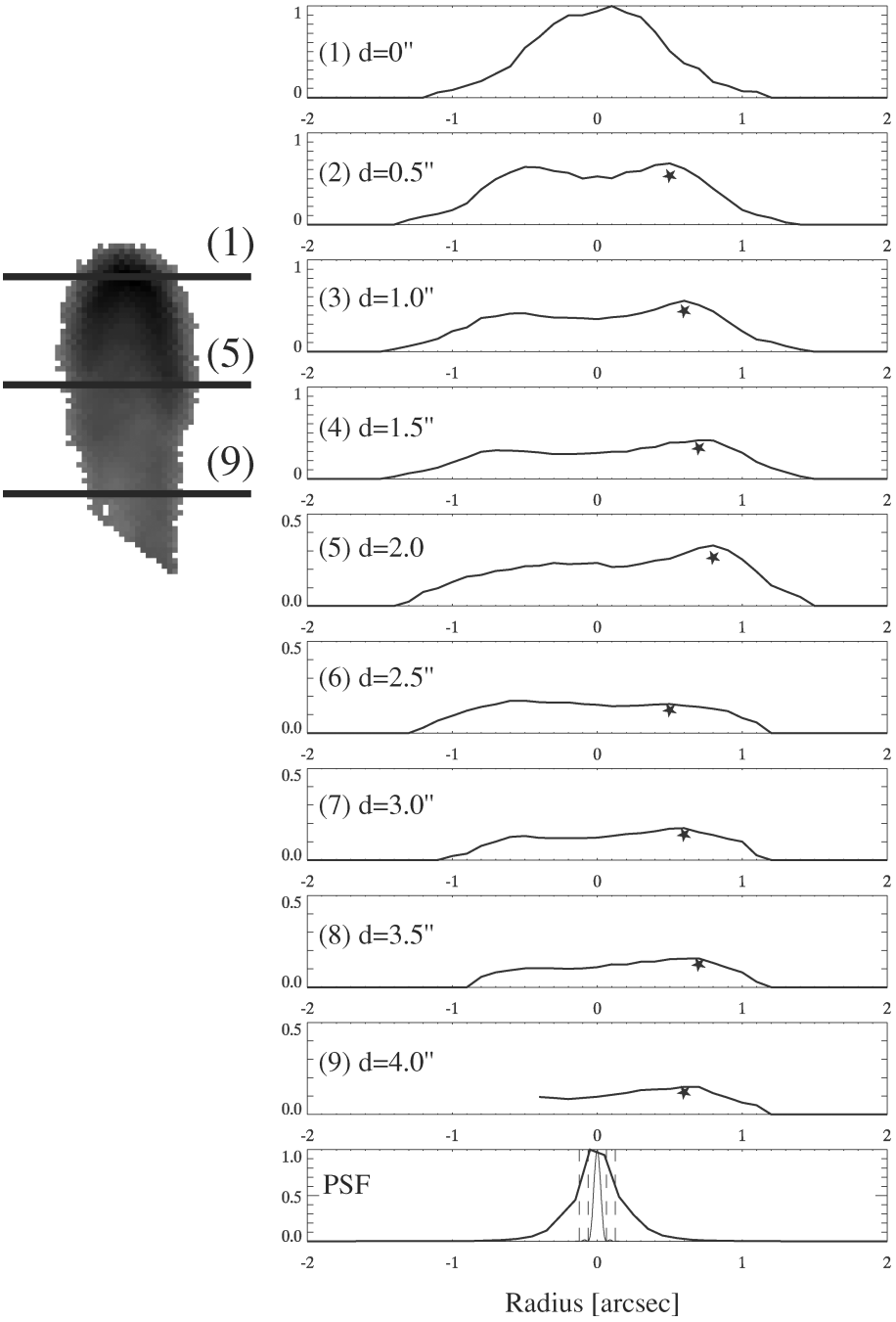

Figure 5. Cross-cut of Fig. 2 along the radial axis, whose intensity is scaled to the maximum intensity of the knot. Approximate locations of cuts are indicated on the left-hand panel. The data are smoothed with a 250-mas bin along the long axis of the knot. The intensity peaks on the east side (right-hand side in this figure) of the knot are marked with the stars in each panel. The bottom panel shows the cross-cut of the telluric standard (bold line), airy disc for 8.2 m circular aperture (thin solid line), and pixel size (125 and 250 mas; thin dashed lines). The spatial resolution is determined by the pixel-scale (sampling rate). The star marks traces that the head is widened until the distance $d = 2.0$ arcsec and then narrowing follows $d > 2.5$. Tail of the PSF is less than 10 per cent of the peak at 0.5 arcsec.

in the absolute H_2 intensity (up to 50 per cent) affects the column density, but not the excitation temperature which is determined by the slope.

3.3 Line-ratio map

Fig. 13 shows the line-ratio maps within the knot. Fig. 13(a) maps the rotational temperature variations within the knot, represented by the 2.03 μm $v = 1$–0 S(2) and 2.12 μm $v = 1$–0 S(1) lines. This rotational temperature is uniform within the errors throughout the knot. This uniform rotational temperature is expected from the energy diagram (Fig. 12), because all of the line intensities follow 1800 K LTE in any area.

The vibrational temperature seems to vary within the knot but this is within the uncertainty. Fig. 13(b) shows the line ratio of 2.24 μm H_2 $v = 2$–1 S(1) and 2.12 μm H_2 $v = 1$–0 S(1). This is the

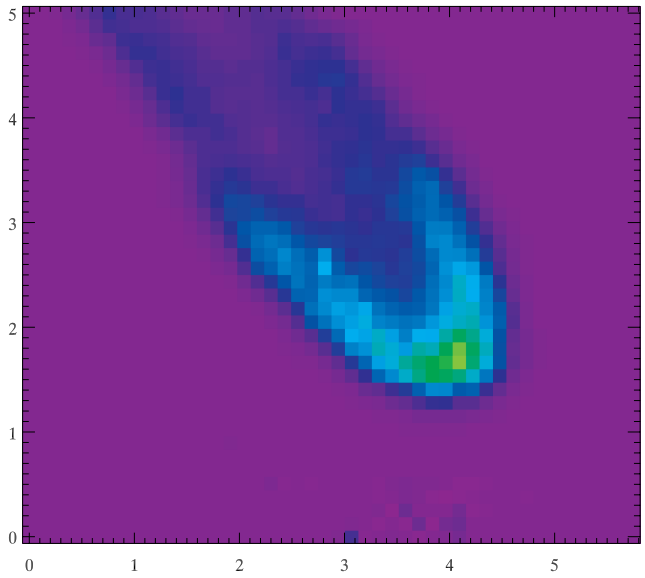

Figure 6. Deconvolved image at 2.12 μm. A faint emitting region at the rim near the crescent is found, as well as narrowing of the tail.

only combination to obtain the vibrational temperature within our observed data. The line ratio tends to be highest at the tip (∼0.1) and to decrease towards the tail, although a careful treatment of $v = 2$–1 S(1) lines is needed.

4 DISCUSSION

4.1 Excitation diagrams and temperatures

The H_2 excitation diagrams are fitted by a single LTE temperature of 1800 K. This is much higher than that of Cox et al. (1998) who obtained 900 K by fitting pure-rotational lines up to the S(7) transition. The region observed by Cox et al. (1998) is located at the western rim of the nebula, and is 5–6 arcmin away from the central star. The pixel size of their ISOCAM data was 6 arcsec and emission from multiple knots contributed to each single pixel. In contrast, our target is a single, isolated knot located at the innermost region of the flock of knots (2.5 arcmin from the central star).

O'Dell, Henney & Ferland (2007) also obtained an excitation temperature of 988 K from 5- to 15-μm spectra in the outer part of the nebula. O'Dell et al. (2007) state that the distance of those slit positions is similar to that of Cox et al. (1998). Although they do not provide detailed information on the slit positions and observing mode for their two *Spitzer* spectra, the *Spitzer* archive can provide this, suggesting that their two slit positions are 5.6 and 4.2 arcmin from the central star, and the slit size is 3.6×57 arcsec^2. Further three spectra at different slit positions are available in the archive, but these do not fit the description of the data in O'Dell et al. (2007).

The difference in measured temperatures suggests that the excitation temperature of H_2 is not uniform within the Helix Nebula: the H_2 molecules reach higher temperatures within the inner region. From about 2.5–5 arcmin away from the central star, the excitation temperature decreases from 1800 to 900–1000 K. This provides evidence for temperature variations within the nebula.

Hora et al. (2006) show that the [3.6]–[4.5] versus [4.5]–[8.0] colour varies within the nebula. All three bands are dominated by H_2 lines. Knots located at the inner rim of the main nebula are

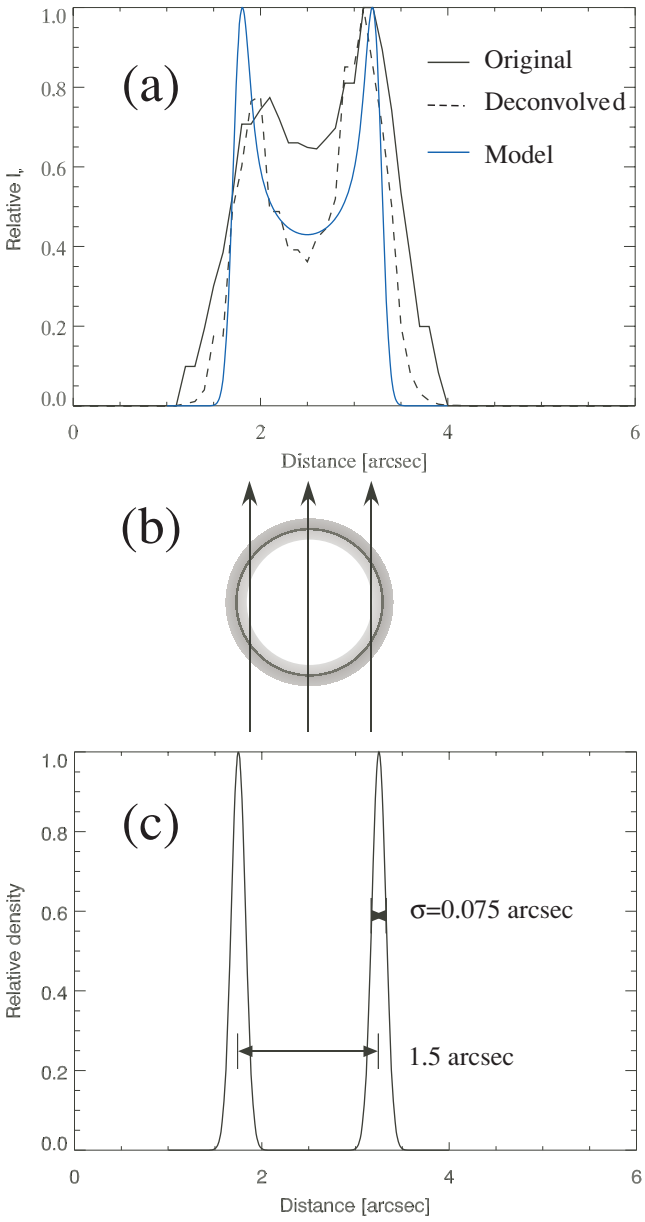

Figure 7. (a) Cross-cut of the observed intensity at 2.12 μm and PSF-deconvolved profile along the radial direction in the head. The intensities are normalized at the peak. The location is 1 arcsec away from the brightest tip. Model profile in panel (a) is to demonstrate a hollow shape in the projected image if the knot is seen from the central star (panel b) with input parameters of the shape (panel c).

brighter in the 4.5-μm band. The strongest expected line in this band is the 4.69 μm H_2 $v = 0$–0 S(9), whose upper energy is the highest among the dominant H_2 lines within the IRAC filters. The colour–colour diagram of Hora et al. (2006) also suggests a higher excitation temperature in the inner region, and global variation in the excitation temperature in the entire nebula. An analysis of spectra with several slit positions within a nebula shows that the H_2 temperature is not uniform within a PN (Hora, Latter & Deutsch 1999; Davis et al. 2003). Excitation temperature variations appear normal within a single PN.

Furthermore, H_2 excitation temperatures in PNe have been found to be as high as 2000 K (Hora et al. 1999; Davis et al. 2003)

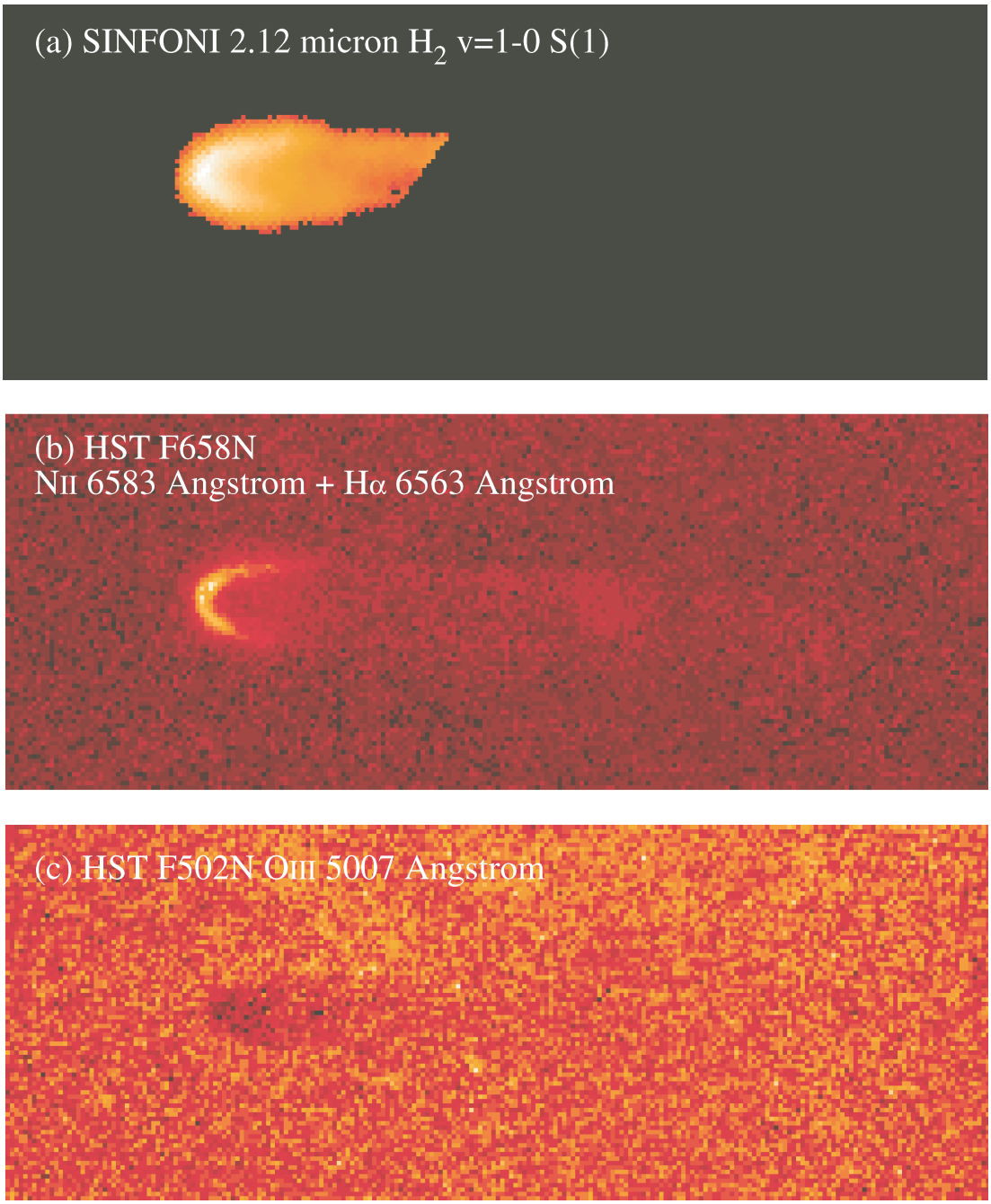

Figure 8. Comparison of the SINFONI 2.12-μm image and *HST* images. The SINFONI and *HST* images were aligned on the tip of the knot. Log intensity scale is used for all of the images. The size of the image is 22.3 × 8.5 arcsec^2.

and lower than 1000 K (Cox et al. 1998; Bernard-Salas & Tielens 2005; Matsuura & Zijlstra 2005a). Variations in excitation temperatures both between PNe and within a single PN appear to be normal.

4.2 Column density

The H_2 line intensities are fitted using column densities in the range of 1×10^{17}–8×10^{17} cm^{-2}. This range is smaller than the Cox et al. (1998) measurements of 3×10^{18} cm^{-2}. Our target is an isolated knot, while the low spatial resolution of the ISOCAM data almost included multiple knots within the field of view, hence the H_2 intensity is much higher (Speck et al. 2002).

The column density of H_2 can be converted to a hydrogen mass of 2×10^{-8} M$_\odot$. Here, we assume that the knot has a column density of 4×10^{17} cm^{-2} (i.e. to emit average intensity over 2 × 2 arcsec^2 at the excitation temperature of 1800 K), the distance is 219 pc, the dimension of the knot is 2 × 2 arcsec^2 and the density is uniform within this area. The estimated hydrogen mass is a factor of 1000 less than the estimate of O'Dell & Handron (1996), who used the extinction of the [O II] line as a mass tracer. Our infrared H_2 lines trace only highly excited H_2, as expected from the upper-state energy

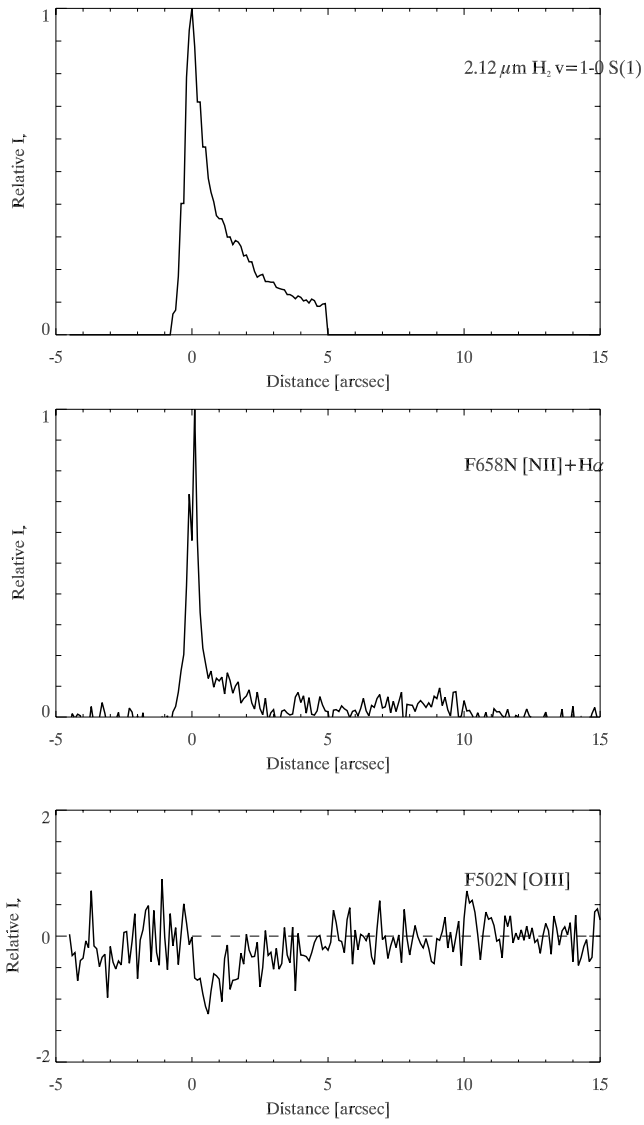

Figure 9. Cross-cut of Fig. 8 along the long axis.

(>6000 K). Colder H_2 gas is inefficient at emitting these lines (Cox et al. 1998).

In order to measure the mass of cold H_2 gas more directly, we need observations at UV wavelengths, where H_2 lines could be found in absorption. However, this approach may be compromised by the contribution to H_2 absorption by the interstellar medium. Adopting the hydrogen mass of O'Dell & Handron (1996) with a comparison of our estimated H_2 mass indicates that H_2 is heated only at the surface, but in fact H_2 is present throughout the knot. This favours a scenario where the detected H_2 was already present within the knot, that is, it is not necessary to assume that it formed from chemical reactions from atomic/neutral hydrogen within this surface. However, this argument is based on an expected correlation between dust extinction and H_2. A direct detection is required to confirm the presence of a large, cold H_2 reservoir.

4.3 Excitation mechanisms of molecular hydrogen

The cometary knot K1 emits a 1–0 S(1) line intensity of 2×10^{-7} W m^{-2} sr^{-1}. The adopted uncertainty is a factor of 2. The 2–1/1–0 S(1) line ratio is $\sim$0.1 $\pm$ 0.02 at the tip, using the uncertainty on the response correction.

Burton, Hollenbach & Tielens (1992) calculated the line intensities of 1–0 S(1) and 2–1 S(1) lines for J-type shocks, C-type shocks and in PDR. We found that within their model the measured line intensities and ratios can be fitted equally well under several model conditions.

(i) A PDR heated by UV radiation where the density is $n = 10^6$ cm^{-3} and the UV strength is $G_0 = 1.2 \times 10^4$ (within the range of $G_0 = 1$–1.2×10^4)

(ii) C-type shocks with an upstream density $n_0 = 10^4$ cm^{-3} and shock velocity $v_s \sim 27$ km s^{-1} (within the range of 27–28 km s^{-1}).

(iii) J-type shocks $n_0 = 10^6$ cm^{-3} and shock velocity $v_s \sim 9$ km s^{-1} (9–10 km s^{-1}).

Although there is some uncertainty in absolute intensity, the line ratio is the strongest constraint on the above conditions.

Meaburn et al. (1998) estimated the molecular hydrogen density of another knot to be 8.9×10^5 cm^{-3} using the extinction in the [O III] 5007 Å line. This knot appears brighter than K1, and larger in radius when observed in the [N II] line. We follow their method to estimate the density of the knot K1. The absorption at [O III] is 0.73 with respect to the continuum (Section 3.1.2). This corresponds to an extinction coefficient $c = 0.15$, $E(B-V) = 0.14$ mag, and an H_2 column density of 4.0×10^{20} cm^{-2}. If the diameter of the knot is 1.5 arcsec, an H_2 number density of 8×10^4 cm^{-3} is obtained for a distance of 219 pc. The derived H_2 density is consistent for the PDR model of H_2 excitation in Burton et al. (1992).

The far-UV (6–13.6 eV) flux at the knot K1 is about $G_0 = 8$, where G_0 is the far-UV radiation measured in units of the Habing (1968) flux. This is based on Su et al.'s (2007) estimate assuming a luminosity of the central star of 76 $L_\odot$ and a distance of 219 pc. The required UV radiation in Burton et al.'s (1992) model is $G_0 > 1 \times 10^4$, which is an order of magnitude higher than the estimated UV radiation field strength at the knot K1. We used the UCL (University College London) PDR model (Bell et al. 2005) to calculate the conditions independently. At a UV radiation field of $G_0 = 8$, we obtain a temperature below 100 K. Röllig et al. (2007) compare benchmark calculations of independent PDR codes, including the UCL-PDR model and Tielens & Hollenbach's (1985) model that was incorporated in Burton et al.'s (1992) H_2 model. They find consistent gas temperatures among PDR models in their benchmark calculations. These results suggest that the PDR models can reproduce the measured LTE gas temperature (1800 K) of the H_2 lines in the knot K1 only, if the UV radiation strength is increased. A similar conclusion is derived by Cox et al. (1997) and O'Dell, Henney & Ferland (2005). The value for G_0 is defined as the flux between 6 and 13.6 Å a narrow-band UV radiation field, adopted for interstellar radiation field. If we consider the continuous stellar spectrum of the central star, the UV flux increases by a factor of 10 (O'Dell et al. 2007). However, this remains a factor of 250 short of the required flux.

The speed of ambient gas for C-type shocks is $v_s \sim 27$ km s^{-1} to fit the H_2 line intensities and line ratios, from theoretical work by Burton et al. (1992). The required velocity can vary by $\sim \pm 10$ km s^{-1} depending on the assumed magnetic field strength and the iron fraction. The [He II] and [O III] lines show an expansion velocity of 13 km s^{-1} near the central star (Meaburn et al. 2005). Within an expanding nebula, hydrodynamic effects will cause significant velocity gradients (Schönberner, Jacob & Steffen 2005), as are observed in PNe (Gesicki, Acker & Zijlstra 2003). The overpressure of the ionized region dominates, and (if present) the pressure

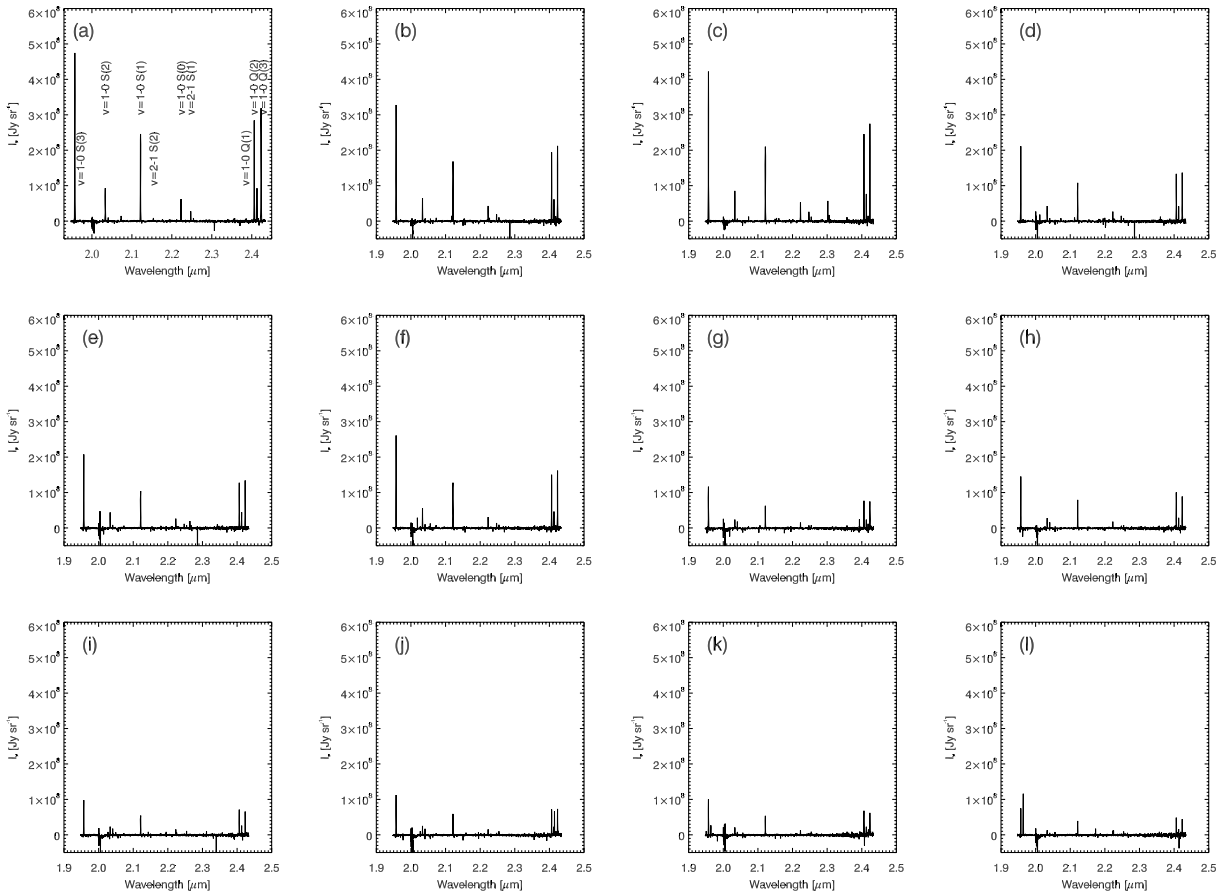

Figure 10. Spectra within the knot K1 at 12 0.675 × 0.5-arcsec^2 areas defined in Fig. 11. The y-axis shows the spectral intensity from -0.5×10^8 to 6×10^8 Jy sr^{-1}. The identifications of the H_2 transitions are indicated in panel (a).

from the inner, hot bubble might be added. The same processes will occur for each knot at the ionized, facing edge. Meaburn et al. (1998, 2005) postulate turbulent velocities $\geqslant$10 km s^{-1} (i.e. larger than the sound speed). A C-type shock velocity could be associated with such motion. The gas density of PNe is typically $n_0 \sim 10^4$ cm^{-3}. This is consistent with the required upstream density. C-type shock excitation of H_2 is possible. Stronger observational constraints on the velocity structure of the knot would be helpful.

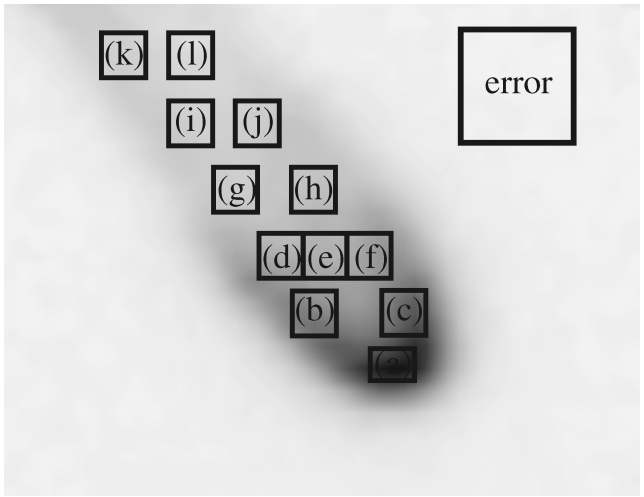

Figure 11. The 12 regions shown by boxes on the 2.12-μm image. The spectra are averaged within that area, which corresponds to the diagram in Fig. 12. The right-hand top box is the area used to estimate the error of the intensities.

The presence of magnetic fields has been reported in several young or pre-PNe using submillimetre polarization (Sabin, Zijlstra & Greaves 2007). They find a magnetic field of ∼1 mG at 5×10^{16} cm from the central star in other PNe. The Helix knots are located 10 times farther from the star than their measured location. A dipole field would decay as r^{-3}: this would leave a negligible field in the Helix Nebula. A solar-type field decays as r^{-2}, and a frozen toroidal field (as favoured by Sabin et al. 2007) may decay slower with radius. The formation of a knot may strengthen after its embedded magnetic field. The field required for the C-type shock is plausible within the knot, compared to the stronger fields detected in more compact shells. The interknot medium is likely to show a weaker field.

An upstream (wind) density of 10^6 cm^{-3} is required for the J-type shock model. Although the density within knots themselves is recorded at 10^6 cm^{-3} (O'Dell & Handron 1996; Meaburn et al. 1998), it is unlikely that the upstream region has such a high density.

5 CONCLUSIONS

We have investigated the detailed structure of a single knot close to the inner edge of the main ring of the Helix Nebula.

Table 2. Intensities of H_2 lines at areas (a)–(c) and ratios with respect to the $v = 2$–1 S(1) line.

Wavelength	Transition	Upper state energy		Statistical weight	Intensity $I_v \times 10^7$ (a)	(b)	(c)	Err[a]	Obs ratio[b] (a)	(b)	(c)
(μm)		(K)	(cm^{-1})		($W\,m^{-2}\,sr^{-1}$)						
1.958	$v = 1$–0 S(3)[c]	8365	5813	33	4.10	2.35	2.96	0.10	220	226	223
2.004	$v = 2$–1 S(4)	14764	10 262	13	<0.40[a]						
2.034	$v = 1$–0 S(2)	7584	5271	9	0.67	0.37	0.49	0.04	36	35	36
2.073	$v = 2$–1 S(3)	13890	9654	33	0.08[d]			0.09	4		
2.128	$v = 1$–0 S(1)	6956	4834	21	1.86	1.04	1.32	0.07	100	100	100
2.154	$v = 2$–1 S(2)	13150	9139	9	0.07[d]			0.08	3		
2.201	$v = 3$–2 S(3)	19086	13 265	33	0.02[d]			0.03			
2.224	$v = 1$–0 S(0)	6471	4497	5	0.42	0.24	0.31	0.06	22	23	23
2.248	$v = 2$–1 S(1)	12550	8722	21	0.18	0.09	0.12	0.04	9	9	9
2.386	$v = 3$–2 S(1)	17818	12 384	21	<0.09[a]						
2.407	$v = 1$–0 Q(1)[c]	6149	4273	9	1.84	1.06	1.30	0.23	99	102	97
2.413	$v = 1$–0 Q(2)[c]	6471	4497	5	0.55	0.29	0.39	0.12	29	28	29
2.424	$v = 1$–0 Q(3)[c]	6956	4834	21	1.85	1.03	1.27	0.14	99	99	96
2.438	$v = 1$–0 Q(4)[c]	7586	5272	9	0.57	0.31	0.38	0.18	30	30	28

[a] 3σ of the noise level of the intensity in the error region indicated in Fig. 11.
[b] Line ratio with respect to the 2.128 μm $v = 1$–0 S(1) line.
[c] These lines have a large (∼30 per cent) error in relative intensity calibration due to the influence of H_2O in the terrestrial atmosphere. They are excluded from the comparison with models.
[d] Marginal detections.

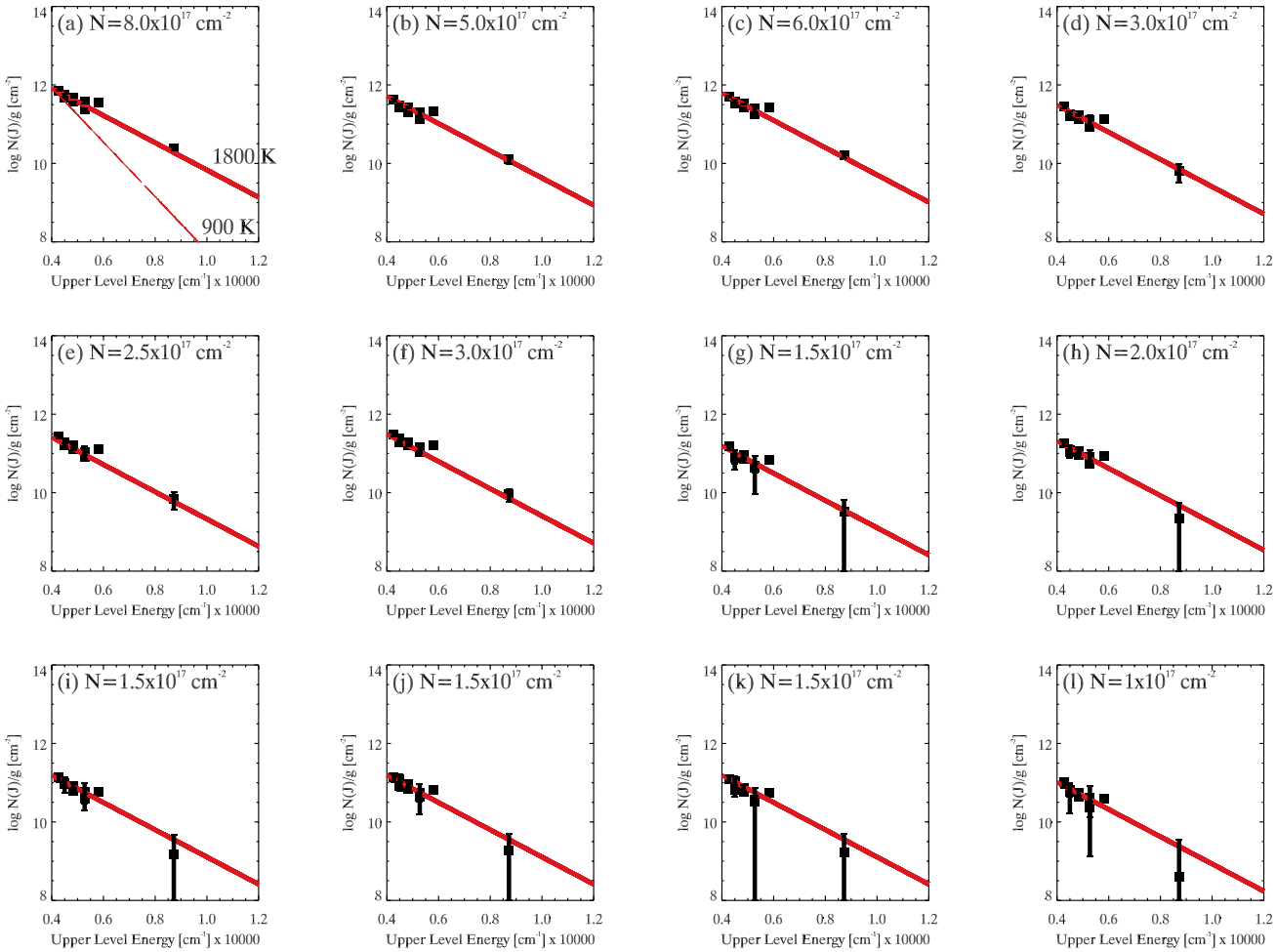

Figure 12. The energy diagrams for area (a)–(l) defined in Fig. 11; the column density for a given J upper level divided by the statistical weight as a function of the upper state energy in cm^{-1}. The square shows the measured energy levels. The thick lines show the LTE case for 1800 K and for column densities as given in the diagrams. For a comparison, we plot the 900 K LTE line, as derived for knots in the outer region of the nebula (Cox et al. 1998) in (a). The column density for the 900 K line is 8×10^{18} cm^{-2}. This temperature cannot fit the H_2 line intensities measured in the knot K1.

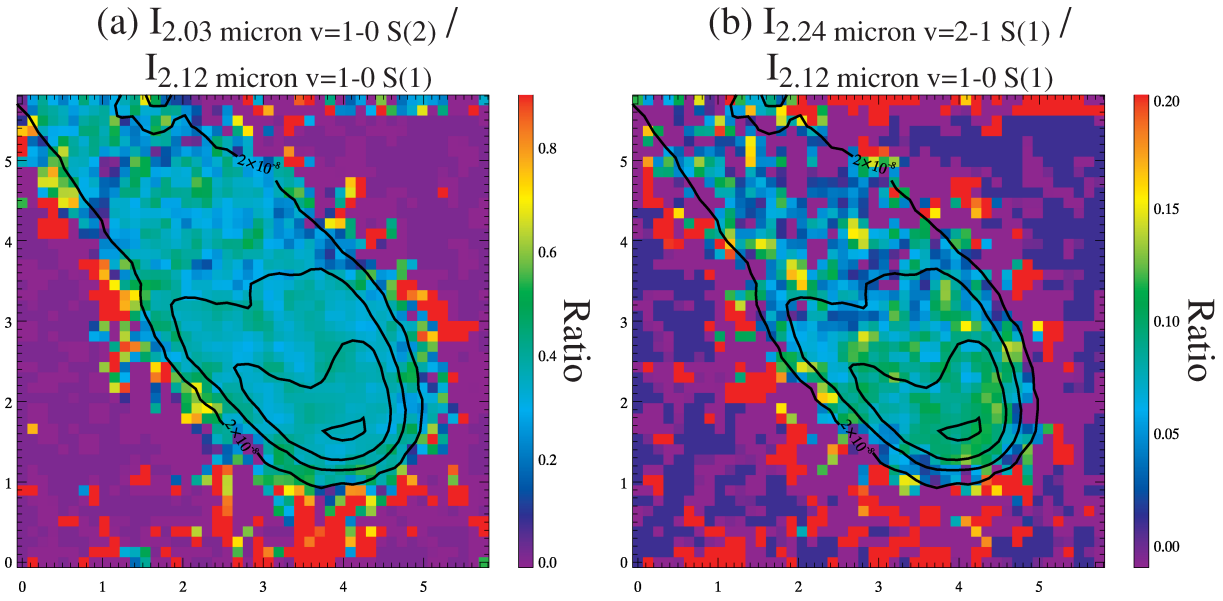

Figure 13. The line-ratio maps of the cometary knot K1. The contour shows the surface brightness of 2.12 μm H_2 $v = 1$–0 S(1) line at 0.2×10^{-7}, 0.5×10^{-7} and 1×10^{-7}, 2×10^{-7} W m^{-2} sr^{-1}.

We find that the rotational-vibrational temperature of H_2 is as high as 1800 K for this innermost cometary knot. The rotational temperature is uniform within the knot, and the vibrational temperature appears to follow the same distribution except for a possible decrease towards the tail. The derived temperature is much higher than previously measured (900 K) for knots in the outer region. The excitation temperature changes with radial distance from the central star. The studied knot has a wide head, with H_2 distributed in a crescent.

We examine the possible molecular hydrogen excitation mechanisms. Based on the line intensities and ratios, C-type shocks can provide a fit using plausible local conditions, although the required velocity is slightly higher than the observed one. This excitation requires the presence of an as-yet-undetected magnetic field. A J-type shock model does not fit. We also tested the possibility that H_2 lines are excited in PDR, but PDR models have difficulties to reproduce the very high temperature, unless the UV field is increased by two orders of magnitude over the stellar radiation field. A further test of the models will require observations of the velocity structure of the head and tail. We also lack a synthesis model combining collisional and UV excitation, with hydrodynamical interactions.

ACKNOWLEDGMENTS

We appreciate technical support from the ESO staff during the observations and the data analysis. MM appreciates encouragement from Prof. Arimoto for this study. MM is grateful for hospitality at the UCL and SAAO during the visits. A discussion with Dr M. Cohen in early stages of this research was very useful.

REFERENCES

Balick B., Frank A., 2002, ARA&A, 40, 439
Beckwith S., Neugebauer G., Becklin E. E., Matthews K., Persson S. E., 1980, AJ, 85, 886
Bell T. A., Viti S., Williams D. A., Crawford I. A., Price R. J., 2005, MNRAS, 357, 961
Bernard-Salas J., Tielens A. G. G. M., 2005, A&A, 431, 523
Black J. H., van Dishoeck E. F., 1987, ApJ, 322, 412
Bonnet H. et al., 2004, The ESO Messenger, 117, 17
Burton M. G., Hollenbach D. J., Tielens A. G. G., 1992, ApJ, 399, 563
Cox P. et al., 1997, A&A, 321, 907
Cox P. et al., 1998, ApJ, 495, L23
Davis C. J., Smith M. D., Stern L., Kerr T. H., Chiar J. E., 2003, MNRAS, 344, 262
Dyson J. E., 2003, Ap&SS, 285, 709
Dyson J. E., Hartquist T. W., Pettini M., Smith L. J., 1989, MNRAS, 241, 625
Dyson J. E., Pittard J. M., Meaburn J., Falle S. A. E. G., 2006, A&A, 457, 561
Eisenhauer F. et al., 2003, Proc. SPIE 4841, 1548
García-Segura G., López J. A., Steffen W., Meaburn J., Manchado A., 2006, ApJ, 646, L61
Gesicki K., Acker A., Zijlstra A. A., 2003, A&A, 400, 957
Habing H. J., 1968, Bull. Astr. Inst. Netherlands, 19, 421
Harris H. C. et al., 2007, AJ, 133, 631
Hora J. L., Latter W. B., Deutsch L. K., 1999, ApJS 124, 195
Hora J. L., Latter W. B., Smith H. A., Marengo M., 2006, ApJ, 652, 426
Hollenbach D., McKee C. F., 1989, ApJ, 342, 306
Hollenbach D., Natta A., 1995, ApJ, 455, 133
Huggins P. J., Manley S. P., 2005, PASP, 117, 665
Huggins P. J., Forveille T., Bachiller R., Cox P., Ageorges N., Walsh J. R., 2002, ApJ, 573, L55
Kaufman M. J., Neufeld D. A., 1996, ApJ, 456, 611
Likkel L., Dinerstein H. L., Lester D. F.Kindt A., Bartig K., 2006, AJ, 131, 1515
McCaughrean M. J., Mac Low M.-M., 1997, AJ, 113, 391
Matsuura M., Zijlstra A. A., 2005a, in Käufl H. U., Siebenmorgen R., Moorwood A. F. M., eds, High Resolution Infrared Spectroscopy in Astronomy. Springer-Verlag, Berlin/Heidelberg, p. 423
Matsuura M., Zijlstra A. A., Molster F. J., Waters L. B. F. M., Nomura H., Sahai R., Hoare M. G., 2005b, MNRAS, 359, 383
Meaburn J., Clayton C. A., Bryce M., Walsh J. R., Holloway A. J., Steffen W., 1998, MNRAS, 294, 201
Meaburn J., Boumis P., López J. A., Harman D. J., Bryce M., Redman M. P., Mavromatakis F., 2005, MNRAS, 360, 963
Meixner M., McCullough P., Hartman J., Son M., Speck A., 2005, AJ, 130, 1784
Modigliani A. et al., 2007, Proc. ADA IV, preprint (astro-ph/0701297)

Natta A., Hollenbach D., 1998, A&A, 337, 517
Neufeld D. A., Dalgarno A., 1989, ApJ, 340, 869
O'Dell C. R., Handron K. D., 1996, AJ, 111, 1630
O'Dell C. R., Henney W. J., Burkert A., 2000, AJ, 119, 2910
O'Dell C. R., Balick B., Hajian A. R., Henney W. J., Burkert A., 2002, AJ, 133, 2343
O'Dell C. R., McCullough P. R., Meixner M., 2004, AJ, 128, 2339
O'Dell C. R., Henney W. J., Ferland G. J., 2005, AJ, 130, 172
O'Dell C. R., Henney W. J., Ferland G. J., 2007, AJ, 133, 2343
Pickles A. J., 1998, PASP, 110, 863
Pittard J. M., Dyson J. E., Falle S. A. E. G., Hartquist T. W., 2005, MNRAS, 361, 1077
Redman M. P., Viti S., Cau P., Williams D. A., 2003, MNRAS, 345, 1291
Röllig M. et al., 2007, A&A, 467, 187
Sabin L., Zijlstra A. A., Greaves J. A., 2007, MNRAS, 376, 378
Schönberner D., Jacob R., Steffen M., 2005, A&A, 441, 573
Speck A. K., Meixner M., Fong D., McCullough P. R., Moser D. E., Ueta T., 2002, AJ, 123, 346
Speck A. K., Meixner M., Jacoby G. H., Knezek P. M., 2003, PASP, 115, 170
Su K. Y. L. et al., 2007, ApJ, 657, L41
Tielens A. G. G. M., Hollenbach D., 1985, ApJ, 291, 747
Turner J., Kirby-Docken K., Dalgarno A., 1977, ApJS, 35, 281
Vishniac E. T., 1994, ApJ, 428, 186
Woods P. M., 2004, PhD thesis, UMIST
Zuckerman B., Gatley I., 1988, ApJ, 324, 501

This paper has been typeset from a TEX/LATEX file prepared by the author.